Bio-inspired Carbon Electro-catalysis for the Oxygen Reduction Reaction

Kathrin Preuss[a,b], Vasanth Kumar Kannuchamy[a], Adam Marinovic[a], Mark Isaacs[c], Karen Wilson[c], Isaac Abrahams[b,d], Maria-Magdalena Titirici[a,b,*]

[a] *School of Engineering and Materials Science, Queen Mary University of London , E14NS, London, UK*

[b] *Materials Research Institute, Queen Mary University of London , E14NS, London, UK*

[c] *European Bioenergy Research Institute, Aston University, B4 7ET Birmingham, UK*

[d] *School of Biological and Chemical Sciences, Queen Mary University of London , E14NS, London, UK*

Abstract

We report the synthesis, characterisation and catalytic performance of two nature-inspired biomass-derived electro-catalysts for the oxygen reduction reaction in fuel cells. The catalysts were prepared via pyrolysis of a real food waste (lobster shells) or by mimicking the composition of lobster shells using chitin and $CaCO_3$ particles followed by acid washing. The simplified model of artificial lobster was prepared for better reproducibility. The calcium carbonate in both samples acts as a pore agent, creating increased surface area and pore volume, though considerably higher in artificial lobster samples due to the better homogeneity of the components. Various characterisation techniques revealed the presence of a considerable amount of hydroxyapatite left in the real lobster samples after acid washing and a low content of carbon (23 %), nitrogen and sulphur (<1 %), limiting the surface area to 23 m^2/g, and consequently resulting in rather poor catalytic activity. However, artificial lobster samples, with a surface area of $\approx$ 200 m^2/g and a nitrogen doping of 2 %, showed a promising onset potential, very similar to a commercially available platinum catalyst, with better methanol tolerance, though with lower stability in long time testing over 10000 seconds.

Key words: Carbonisation, Biomass-derived Carbons, Oxygen Reduction Reaction, Fuel Cells, Electro-catalysis

*** Corresponding author.** m.m.titirici@qmul.ac.uk

1. Introduction

The increasing trend in oil price, concerns about energy security and the need for improvement of hydrogen infrastructure has sparked a flurry of research into the technological aspects of its production and distribution. Fuel cells are considered as one of the most promising technologies, providing clean and sustainable energy. A fuel cell`s efficiency is mainly dictated by the efficiency of the catalyst for the oxygen reduction reaction (ORR), which occurs at the cathode of the fuel cell. Up to this point, platinum supported on carbon materials has proven to be the best catalyst for the ORR, though certain shortcomings still limit the large-scale commercialisation of fuel cells. The rather slow ORR kinetics and low durability/stability in terms of long term usage as well as the very limited resource of platinum and thus the

high cost make the accessibility of this technology limited [1], [2]. Hence, there is a high demand for alternative inexpensive catalyst materials, with good ORR performance similar to platinum.

Carbon based materials are considered as promising alternative candidates due to their excellent electronic and mass transport properties [3], which are essential for the ORR process. Within this context, nitrogen doped carbons have become popular and are often reported as very well performing ORR catalysts [4]. Theoretically, the electronic transport properties and thus the ORR efficiency of the carbon material depend on the nature of the nitrogen atom incorporated in the carbon framework [5]. The majority of studies have involved incorporation of nitrogen atoms either via in situ doping [6],[7],[8], or by the post-treatment of an already synthesised carbon material [9],[10]. In situ doping has proven to be the preferential route to obtain homogeneously distributed nitrogen atoms in the carbon framework. To achieve this, usually a nitrogen source is introduced in the synthesis process along with the carbon source in the presence of an activation agent or pore generating compound (inorganic salts) at elevated temperatures [11],[12]. The activation agent or "template" is usually added to create high surface area and pore volume, which are both essential features for the ORR [13]. Synthesising ORR catalysts from biomass is a further improvement, as it can make the process more sustainable and considerably reduce the production costs.

The second most abundant biomass after cellulose as well as the most abundant nitrogen containing compound in nature is chitin [14]. Chitin can be found in crustacean shells as the main component together with calcium carbonate, which is needed for strengthening, aside from various proteins [14]. The worldwide consumption of crustaceans in 2013 alone was 13 Mt [15], making chitin, as well as its deacetylated derivative chitosan readily available biomass sources for various applications, such as water treatment, pharmaceutical or cosmetic products and plant protection [16].

Several catalysts for electrochemical applications synthesised from chitin and chitosan have been reported in the literature with promising features for the ORR. Yuan et al. [17] carried out hydrothermal carbonisation of pure chitin mixed with water followed by high temperature activation with $ZnCl_2$, resulting in carbon sheets with a very similar onset potential to standard platinum in alkaline media. Li et al. [18] synthesised a chitin aerogel from shrimp shells via various acidic and alkaline washing steps, followed by pyrolysis, which showed an even slightly more positive onset potential than commercial platinum on carbon, with an impressive stability and methanol tolerance. Wu et al. [19] used chitosan as a starting material in a two-step process, where first chitosan and acetic acid were hydrothermally carbonised followed by pyrolysis. The catalytic performance was similar to that for the chitin aerogel [18]. Additionally Wu et al. co-doped their catalyst with sulphur, which led to a further increase in activity and to an identical onset potential to the platinum standard. Nitrogen doped carbon nanosheets with good catalytic activity in alkaline media have also been synthesised from a chitosan and melamine mixture with a pyrolysis process followed by KOH activation [20]. Wu et al. [21] synthesised a catalyst from pure chitosan with rather low catalytic activity, that showed excellent performance and stability when a cobalt salt was added during the synthesis process, resulting in an interconnected nitrogen doped carbon framework with Co/Co_3O_4 nanoparticles. A different approach was taken by Aghabarari et al. [22], who

used a chitosan derivative mixed with carbon black as support for platinum particles to show enhanced catalytic activity compared to the commercial platinum supported on carbon black.

Though a considerable amount of research has been carried out in the field of catalysts made from chitin and chitosan, our aim was to find an easy and straightforward one-pot approach, without the need for several process steps or harsh chemicals. Herein we report the synthesis of a catalyst made purely from food waste, i.e. lobster shells taken from the lobster's carapace, as this part contains the largest amount of chitin, in relation to calcium carbonate [23]. However, a particular concern when using real biomass is the reproducibility in the resulting materials due to the very heterogeneous structure of the biomass (i.e. not all lobster shells contain the same type and amount of chitin and $CaCO_3$). Therefore, a simplified version of artificial lobster shell, made of chitin and calcium carbonate, was also synthesised and tested as a catalyst for ORR for comparison.

2. Experimental

2.1. Catalyst synthesis

All chemicals were used as received from Sigma Aldrich in pure form. Frozen lobster shells (*Homarus americanus*) taken from the animals` abdomen after consumption of the lobster meat, were used to produce the lobster catalyst (abbr. L). A paste made out of 1.5 g Chitin and 0.5 g $CaCO_3$ with 7 mL of deionized water, which was dried at room temperature overnight, represents the simplified artificial lobster (abbr. AL). Both catalysts were weighed into ceramic crucibles, closed with a ceramic lid and placed in a Carbolite high temperature furnace, followed by flushing with nitrogen for 30 minutes. The carbonisation was carried out under inert atmosphere with a heating rate of 3 ^{o}C/min up to 1000 ^{o}C, where the temperature was kept for 4 hours. The samples were then allowed to cool to room temperature under inert atmosphere. To remove residues like calcium carbonate from both samples, washing in 3 M acetic acid was performed, by stirring for 24 hours, followed by rinsing with deionized water over vacuum filtration and freeze drying for 48 hours.

2.2. Catalyst characterisation

Electron micrograph images were obtained with a FEI Quanta 3D Scanning Electron Microscope (SEM), including Energy-dispersive X-ray spectroscopy (EDS), and a JEOL JEM-2010 Transmission Electron Microscope (TEM). Elemental Analysis of C, H, N and S was performed with a Thermo Flash 2000 analyser fitted with a Cu/CuO CHNS column and a TCD detector, calibrated to sulphanilamide. Functional surface groups were specified via X-ray Photoelectron Spectroscopy (XPS) using a Kratos Axis HSi XP spectrophotometer equipped with a charge neutraliser and a monochromated Al K_α source (1486.7 eV). Spectra were recorded at normal emission using a pass energy of 40 eV under a vacuum of 10^{-10} Torr. Surface area and pore size distribution were determined with Brunauer-Emmett-Teller (BET) theory and Quenched Solid Density Functional Theory (QSDFT), respectively, using nitrogen absorption and desorption isotherms obtained at 77 K with a Quantachrome Nova 4200e. Thermogravimetric analysis

(TGA) was carried out on a TA Instruments Q500 with a heating rate of 10 ºC/min up to 1000 ºC in Air. Raman spectroscopy was performed with a Renishaw Raman microscope with a helium neon laser at 633 nm.

Electrochemical testing was performed with a rotating (RDE) and a rotating ring (RRDE) disk electrode on a Metrohm Multi Autolab M101. A three-electrode configuration with Ag/AgCl as reference electrode and platinum as counter electrode was used, as well as a 3mm diameter glassy carbon (GC) working electrode for RDE and a 5 mm diameter GC disk with platinum ring for RRDE, respectively. Samples were tested in alkaline and acidic media at room temperature, using 0.1 M KOH and 0.5 M H2SO4, respectively. The samples` performance was compared to a commercially available platinum standard from Sigma Aldrich (20 wt% platinum on Vulcan carbon). The mass loading for the synthesised catalysts on the electrodes was kept at 212 μg/cm2 and 107 μg/cm2 for the platinum standard. Testing was performed by Cyclic voltammetry (CV) at a scan rate of 100 mV/s was run after first purging the electrolyte with N_2 for 30 minutes. This was, followed by purging with O_2 for another 30 minutes and subsequently carrying out CVand Linear Sweep Voltammetry (LSV) at a scan rate of 10 mV/s for rotation speeds ranging between 400 and 2400 rpm. For stability/durability testing a chronoamperic profile was run for 10000 seconds, where a constant potential of -0.25 V was applied at a constant rotational speed of 800 rpm and the change in current was recorded. To check the samples` tolerance to methanol, a chronoamperic profile was run, where 5 mL of methanol was added to the electrolyte after 160 seconds. For the electrochemical testing an ink of each catalyst was prepared by dissolving either 3 mg for the synthesised catalysts or 1.5 mg of the platinum standard in 100 μL Nafion (5 %w/w in water and 1-propanol, Alfa Aesar) and 900 μL deionized H_2O, leaving the mixture to sonicate for at least 30 minutes to ensure homogenisation. Subsequently 5 μL (RDE, electrode area 0.071 cm^2) or 14 μL (RRDE, electrode area 0.196 cm^2) of the ink was carefully pipetted on the working electrode and dried at room temperature.

Electron transfer numbers for the RDE were calculated by the Koutecky-Levich equation:

$$\frac{1}{j} = \frac{1}{j_k} + \frac{1}{j_l} = \frac{1}{nFAkC} + \frac{1}{0.62nFAD^{\frac{2}{3}}\omega^{\frac{1}{2}}\nu^{-\frac{1}{6}}C}$$

Where j represents the measured current density, j_k and j_l are the kinetic and the diffusion-limited current densities, respectively. The electron transfer in the oxygen reaction is described by n, F is the Faraday constant (96485 C/mol), A is the electrode area, k is the rate constant for the oxygen reduction, D is the diffusion coefficient of oxygen in the electrolyte (1.9×10^{-5} cm^2/s), ω is the angular velocity of the electrode, ν is the kinematic velocity of the electrolyte (0.01 cm^2/s) and C is the concentration of saturated oxygen in the electrolyte (1.2×10^{-3} mol/L). The number of electrons transferred during the oxygen reduction can then be calculated by the slope, when plotting $\frac{1}{j}$ vs. $\frac{1}{\omega^{\frac{1}{2}}}$.

Measurements with an RRDE were obtained with a Pt ring and GC disk electrode. To calculate the electron transfer number and the H_2O_2 yield, the measured currents on the disk I_D and the ring I_R and the collection efficiency N of the Pt ring (25 %) were used.

$$\%(\boldsymbol{H_2O_2}) = \mathbf{200} \times \frac{\boldsymbol{I_R/N}}{\boldsymbol{I_D + I_R/N}}$$

$$\boldsymbol{n} = \mathbf{4} \times \frac{\boldsymbol{I_D}}{\boldsymbol{I_D + I_R/N}}$$

3. Results and discussion

3.1. Physical characterisation

Two biomass-derived electro-catalysts were synthesised, one from real lobster shells (abbr. L), the other from chitin and calcium carbonate (abbr. AL), representing a simplified model of artificial lobster. Figure 1 shows surface areas and pore size distributions, obtained via nitrogen sorption isotherms with BET and QSDFT. Values for the surface area as well as for the pore volume can be found in Table 1. For both samples the surface area increases after the acidic treatment with 3 M acetic acid, due to the removal of calcium carbonate and other impurities. With 23 m^2/g after the acid treatment L has a rather low specific surface area. However, AL shows a considerably higher surface area around 188 m^2/g, with a high amount of micro-, but also mesopores, which can be explained by the use of $CaCO_3$. Calcium carbonate as a pore agent has been well studied and reported in the literature [24,25]. During the pyrolysis process, calcium carbonate decomposes to calcium oxide and carbon dioxide, the latter can oxidise carbon to yield CO. In addition, at elevated temperatures (>700 °C), $CaCO_3$ can react with the nitrogen atoms in chitin to form an unstable compound $Ca(CN)_2$, which can further decompose to $CaCN_2$ and C [24]. This essentially creates a large number of micropores and mesopores, depending on the precursor (artificial or natural lobster) as well as the temperature conditions. The distinct difference in surface area of the two catalysts might be explained by the uneven distribution of $CaCO_3$ in the real lobster sample as well the presence of proteins and other impurities which stabilize the surface of $CaCO_3$ and thus limit the pore formation during pyrolysis. In contrast, when $CaCO_3$ is homogeneously mixed with chitin in the artificial lobster sample, and no other elements are present and pore formation is no longer hindered.

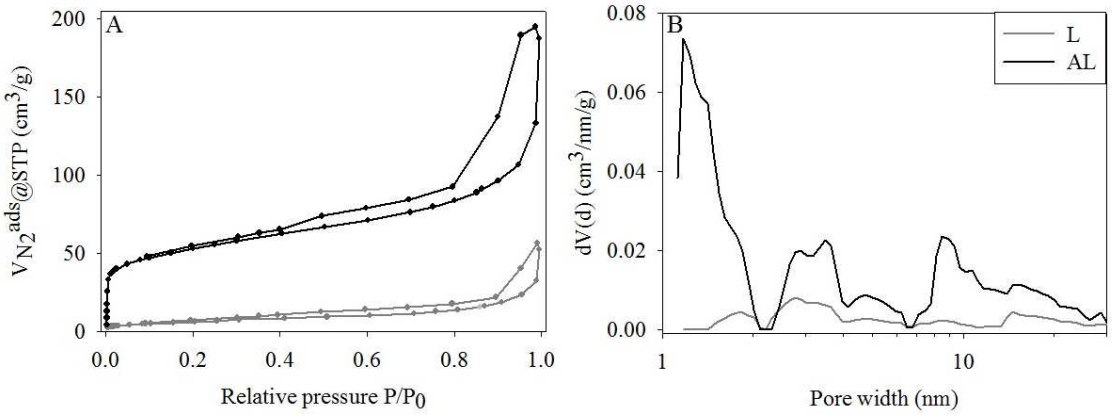

Figure 1. (A) Nitrogen sorption isotherms and (B) pore size distribution for Lobster/L (grey) and Artificial Lobster/AL (black) after the acid treatment.

Table 1. Surface area and pore volumes for Lobster/L and Artificial Lobster/AL determined via BET and QSDFT from nitrogen sorption isotherms.

Sample	Surface area (m^2/g)	V_{tot} (cm^3/g)
L (before acid treatment)	10	0.043
L	23	0.067
AL (before acid treatment)	63	0.142
AL	188	0.285

The difference in surface areas and porosity correlates well with the electron micrographs in Figure 2 and 3. SEM images show a similar morphology for both samples, consisting of agglomerated unevenly distributed spheres and web like structures as well as bigger fragments. Though the surface properties of these fragments seem to be different for the two samples, with a rather even surface for L and a creased surface in AL. Transmission electron microscopy showed a homogeneous structure of porous carbon for AL, with a very typical shape/formation when $CaCO_3$ has been used as pore agent [24,25], made up of connected particles with a shell. In contrast, L consists of a variety of carbon morphologies, some thin sheets with a web-like structure, as well as an interconnected particle network (Figure 3C) similar to AL. Additionally, there are some larger crystals present, which may be attributed to leftover calcium carbonate [26] or hydroxyapatite [27]. The presence of calcium and phosphorus was verified via EDS and XPS (Figure 4 and 5) and will be discussed further on.

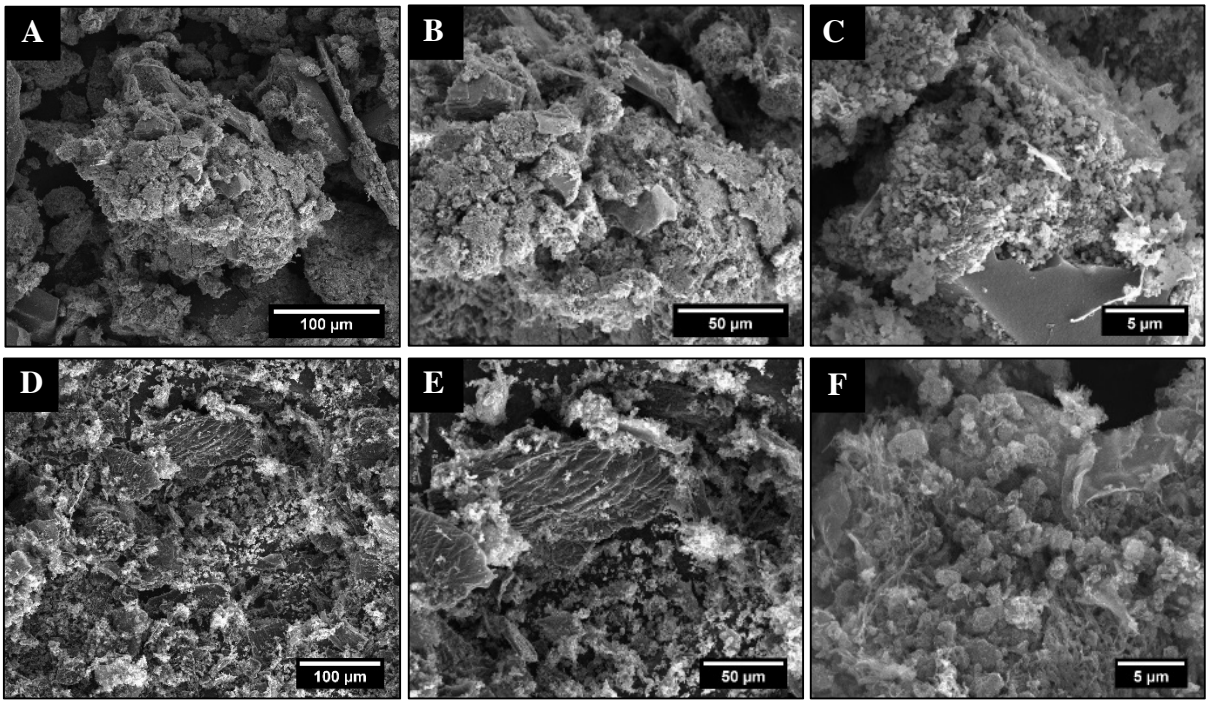

Figure 2. Scanning electron micrographs of A, B, C) Lobster/L and D, E, F) Artificial Lobster/AL.

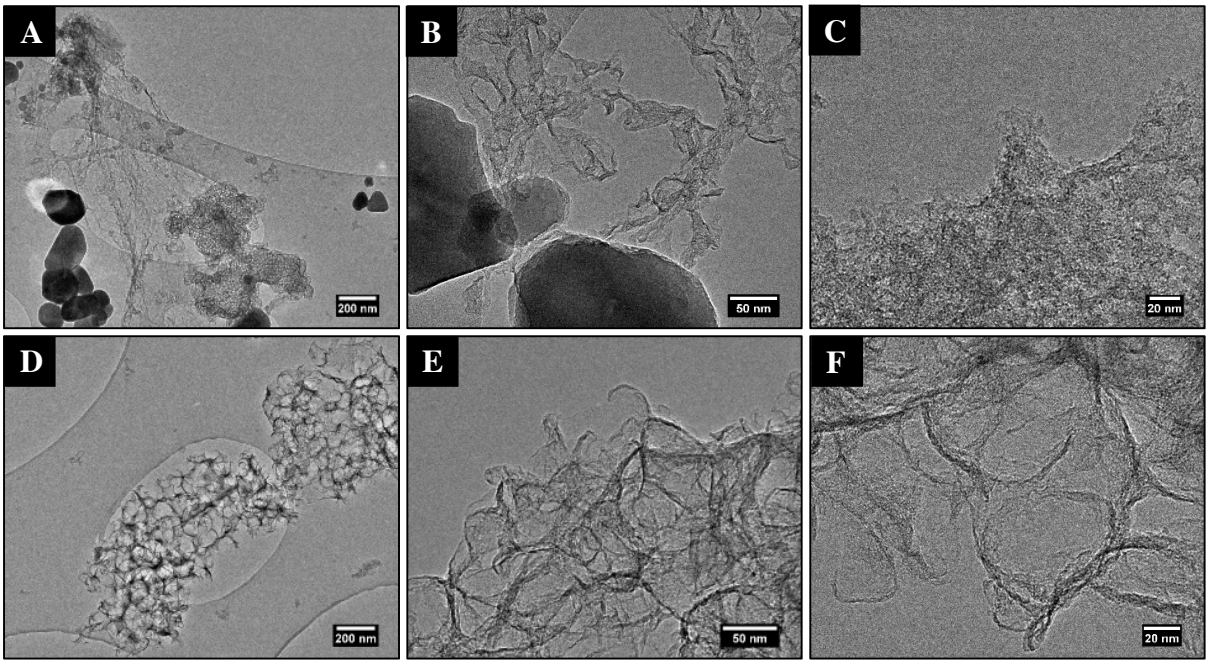

Figure 3. Transmission electron micrographs of A, B, C) Lobster/L and D, E, F) Artificial Lobster/AL.

To determine which elements are present in both samples, Energy-dispersive X-ray spectroscopy (EDS) was performed during SEM (Figure 4). Residues of calcium were found in both catalysts, indicating that the washing step with acetic acid may have been insufficient, either in process time or concentration of the acid. Furthermore carbon, oxygen and nitrogen could be found in both samples, as well as sulphur and phosphorus in L, which may derive from the proteins present in lobster shells. Overall, C, O, N and Ca seem to be distributed homogeneously throughout the analysed area in AL, with the intensities decreasing in the order of C > O > N > Ca. For L oxygen, nitrogen and sulphur seem to be evenly distributed throughout the analysed area, while carbon is mostly present in the large fragments, calcium and phosphorus (most likely forming hydroxyapatite) are more distributed in the smaller parts with an uneven, sponge like surface.

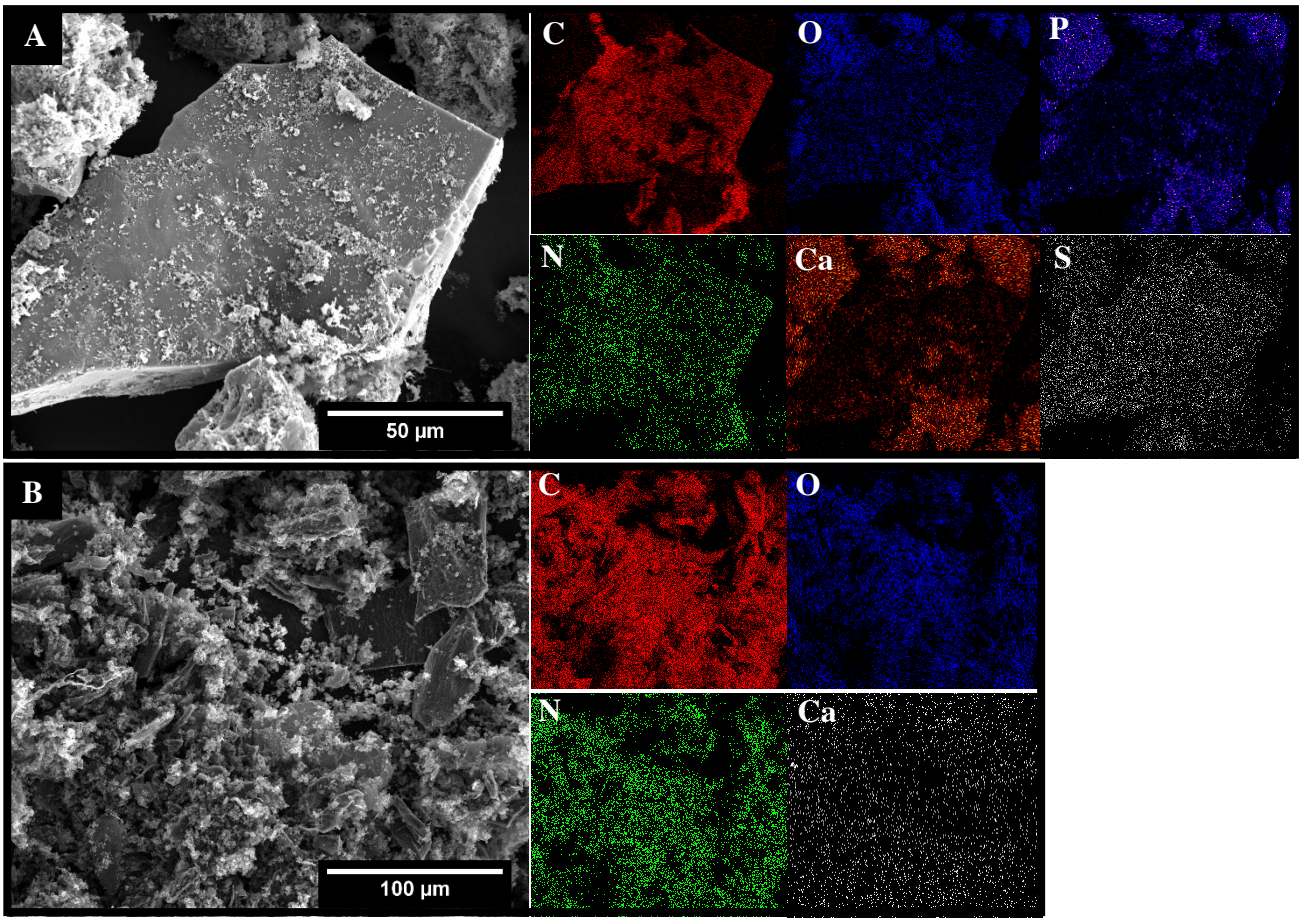

Figure 4. Energy-dispersive X-ray spectroscopy for A) Lobster/L showing the presence of carbon, oxygen, nitrogen, calcium, phosphorus and sulphur and B) Artificial Lobster/AL showing carbon, oxygen, nitrogen and calcium.

For a more accurate understanding of the sample`s composition, elemental analysis was carried out to determine the amounts of C, H, N and S, as summarised in Table 2. With only 23 wt% L has a rather low amount of carbon, considering the carbonisation at 1000 °C; hydrogen, nitrogen and sulphur are all also considerably low (< 1 wt%). These rather low concentrations may be explained by the fact, that real lobster shells contain a considerably high amount of calcium carbonate and other impurities in relation to the concentration of chitin [23]. However, AL shows a more typical amount of carbon with 82 wt% and a higher concentration of nitrogen (2 wt%), which may be due to the higher ratio of chitin to $CaCO_3$. XPS spectra (Figure 5) also revealed the presence of calcium and phosphorus for L, indicating the presence of hydroxyapatite ($Ca_5(PO_4)_3(OH)$). Both samples show a very low concentration of nitrogen in bulk analysis (EA) as well as in the surface analysis (XPS). Due to the high temperature (1000 °C) during the carbonisation, nitrogen is expected to occur mostly in graphitic, but also in pyridinic state [28],[29]. Two peaks can be attributed for graphitic nitrogen and pyridinic N-oxide in the N 1s spectra of L (Figure 5B) around 401 and 405 eV, respectively [8],[30], though interpretation of the nitrogen species at such low concentrations (>1 wt%) may not necessarily be reliable due to high noise. Pyridinic N-oxide may have been formed from pyridinic N due to the treatment with acetic acid. With a higher nitrogen content, AL shows two peaks in the N 1s spectra around 400.7 and 398.2 eV which can be attributed to 73.5 %

graphitic and 26.5 % pyridinic nitrogen, respectively [7].

Table 2. Elemental composition determined via EA (wt%) and XPS (*at*%) for Lobster/L and Artificial Lobster/AL.

Sample	C	H	N	S
L	23.25	0.27	0.42	0.54
	46.39	-	*0.96*	*0.82*
AL	82.14	0.59	2.08	-
	92.1	-	*3.67*	

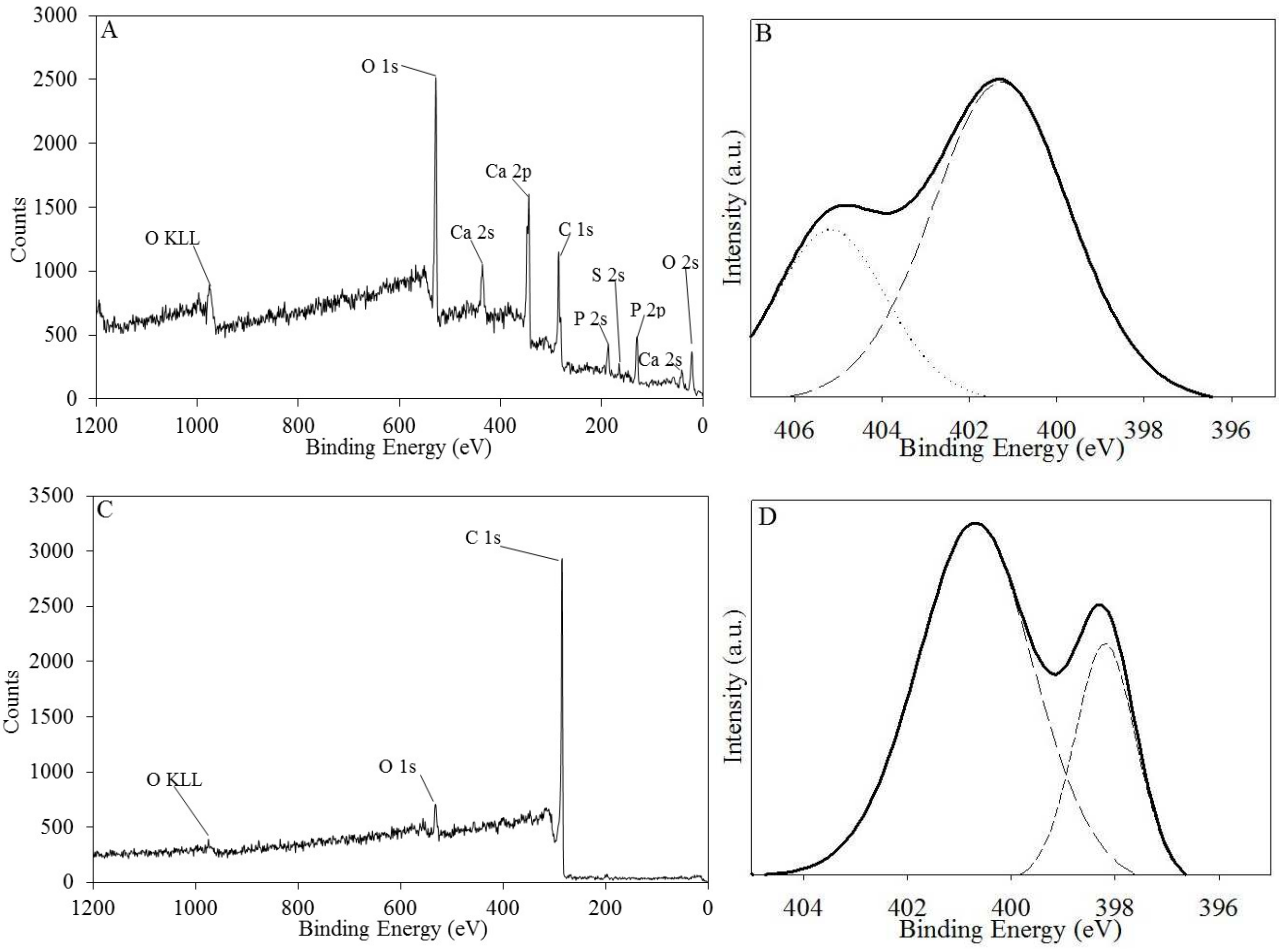

Figure 5. XPS survey spectra for A) Lobster/L and C) Artificial Lobster/AL. Deconvoluted N1(s) photoelectron envelopes of B) Lobster/L and D) Artificial Lobster/AL.

Raman spectroscopy was carried out at an excitation wavelength of 633 nm, both samples show the characteristic D- and G-band peaks around 1330 and 1580 cm^{-1}, respectively [31]. While the peaks for L occur at 1329 and 1592 cm^{-1}, a slight blue shift (higher frequencies) are seen in AL with values of 1334 and 1584 cm^{-1}, respectively, which is apart from the characteristic D band another measure for defects. The

ratio of D to G bands can be used to investigate the level of disorder or the sp^2/sp^3 ratio in carbon, respectively. I_D/I_G for L is 2.48 and slightly less at 2.21 for AL. Higher I_D/I_G values can be attributed to more numerous, but smaller sp^2 graphitic domains present as well as the existence of defects [32]. The rather broad peak between 2600-3200 cm^{-1} can be seen as an overlay of the 2D, D+G and 2D` disorder peaks [33], indicating that both samples are well carbonised with some graphitic domains, though slightly better for AL due to the higher intensity. Additionally a small peak occurs in the spectrum for L at 960 cm^{-1}, which can be attributed to the presence of hydroxyapatite [34], [35].

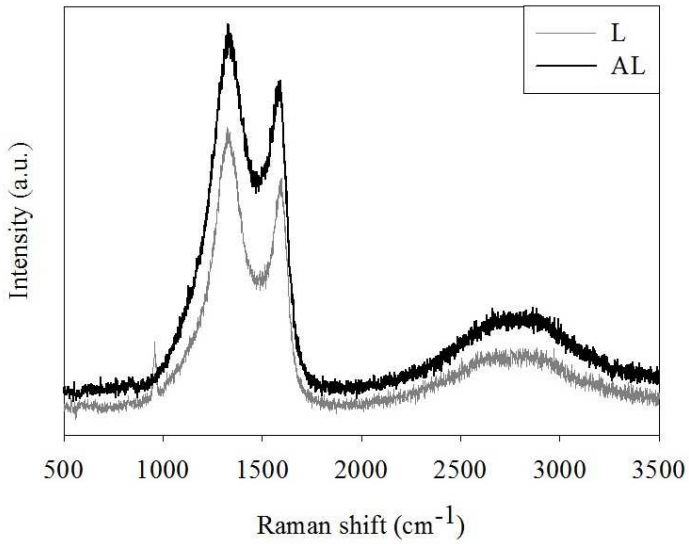

Figure 6. Raman spectra performed at an excitation wavelength of 633 nm for Lobster/L (grey) and Artificial Lobster/AL (black).

Thermogravimetric analysis was performed in air for both samples. The initial weight loss can be attributed to the loss of water still remaining in both materials, followed by the combustion of organic matter around 470 °C. Only 5.9 % of the initial weight of AL remained after the thermogravimetric analysis, indicating that most of its content was organic matter, such as carbon and nitrogen. However, 76.6 % of L remained after the temperature treatment, which is in good agreement with the results obtained via elemental analysis (Table 2). After the thermogravimetric analysis a considerable amount of a white powder was recovered in the case of L, again confirming the presence of hydroxyapatite.

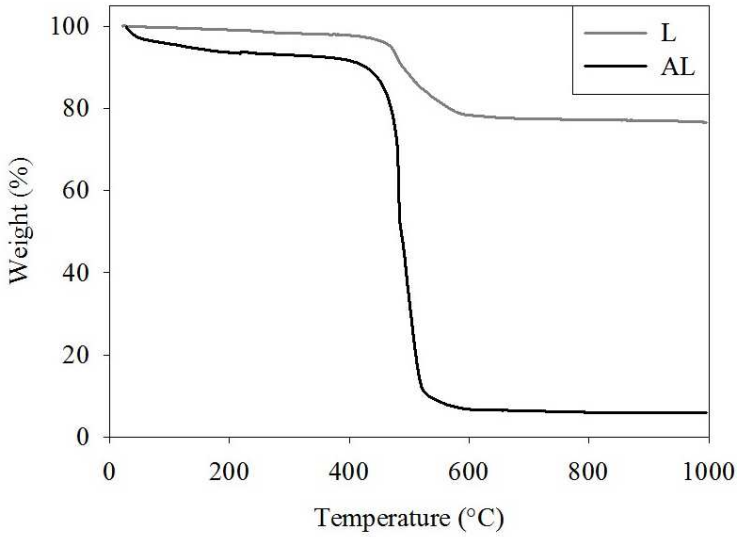

Figure 7. Thermogravimetric analysis of Lobster/L (grey) and Artificial Lobster/AL (black) in air with a heating rate of 10 °C/min.

3.2. Electrochemical characterisation

The synthesised catalysts were tested in an electrochemical setup to determine their catalytic activity. Cyclic voltammetry (CV) was performed in 0.1 M KOH and 0.5 M H_2SO_4 at a scan rate of 100 mV, both in nitrogen and oxygen saturated electrolyte (Figure 8). Both catalysts show the characteristic peak for the oxygen reduction reaction, though the artificial lobster seems to perform better in terms of onset potential and kinetics. This is also confirmed via linear sweep voltammetry (LSV) in 0.1 M KOH and 0.5 M H_2SO_4 at a scan rate of 10 mV, also shown in Figure 8, which also contains data for the platinum standard (20 wt% platinum on Vulcan carbon). AL shows a very similar onset potential compared to the platinum standard in alkaline media, whereas the L has a far more negative onset potential, suggesting it to be an unsuitable candidate for electro-catalysis. The limiting current though is considerably less for AL than for the platinum standard. In acidic media, both catalysts show none to very little activity, no peak for the oxygen reduction reaction can be detected in the cyclic voltammograms, the onset potential for AL compared to the platinum standard is negligibly low. This distinct difference in performance in alkaline and acidic media is often reported for metal free carbon catalysts and can be explained by the inhibition effect from the strong anion adsorption, which is considerably less in alkaline than acidic solution due to the fact that only OH anions are present in alkaline conditions [36].

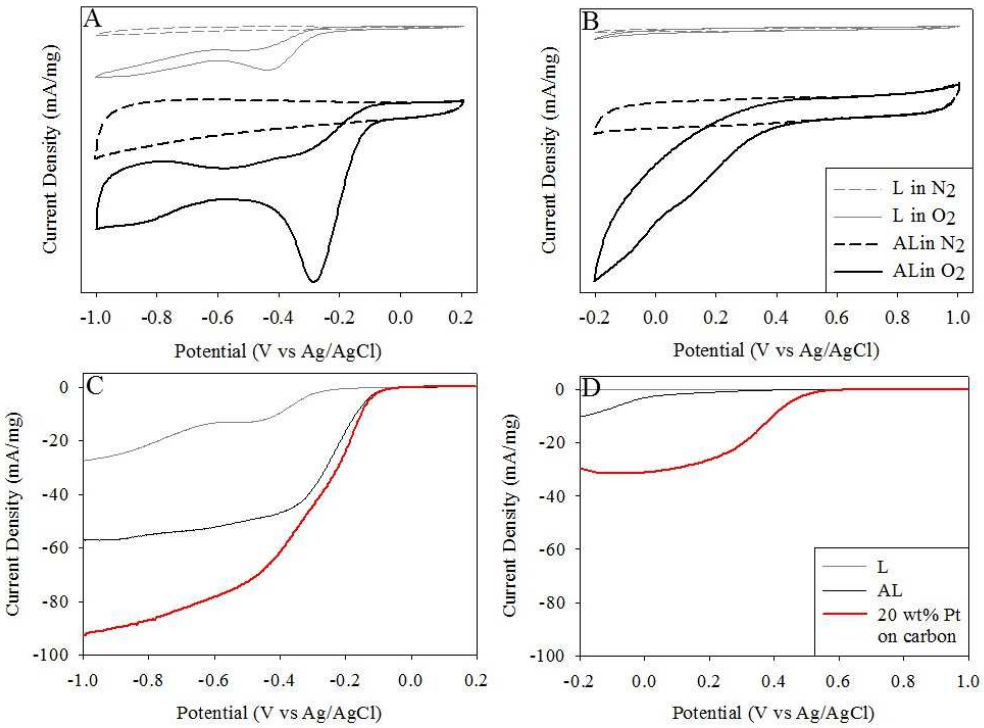

Figure 8. Cyclic voltammograms for Lobster/L (grey) and Artificial Lobster/AL (black) in A) 0.1 M KOH and B) 0.5 M H_2SO_4 either saturated with nitrogen (dotted lines) or oxygen (full lines) recorded with a RDE setup. Comparison of the RRDE polarisation curves at 1600 rpm for Lobster/L (grey), Artificial Lobster/AL (black) and 20 wt% platinum on Vulcan carbon (red) in C) 0.1 M KOH and D) 0.5 M H_2SO_4.

The electron transfer number was calculated for both samples in alkaline media with RDE in the potential range of -0.4 V and -0.6 V. L shows an average electron transfer number of 2.7, whereas AL shows a promising electron transfer number of 4.0. For a more precise idea about which pathway is favoured by the catalyst, the electron transfer numbers were additionally calculated from the measured ring and disk currents of the RRDE and are plotted together with the hydrogen peroxide yield in Figure 9. L seems to proceed via a mixture of the two and four electron pathways, though mostly the two electron pathway with a considerable amount of H_2O_2 formed. Whereas AL, though still proceeding via a mixture of the two pathways, seems to take mostly the four electron pathway, with only a maximum of 20 % H_2O_2 yield, still distinctly higher than the commercially available platinum catalyst with a yield below 10 %.

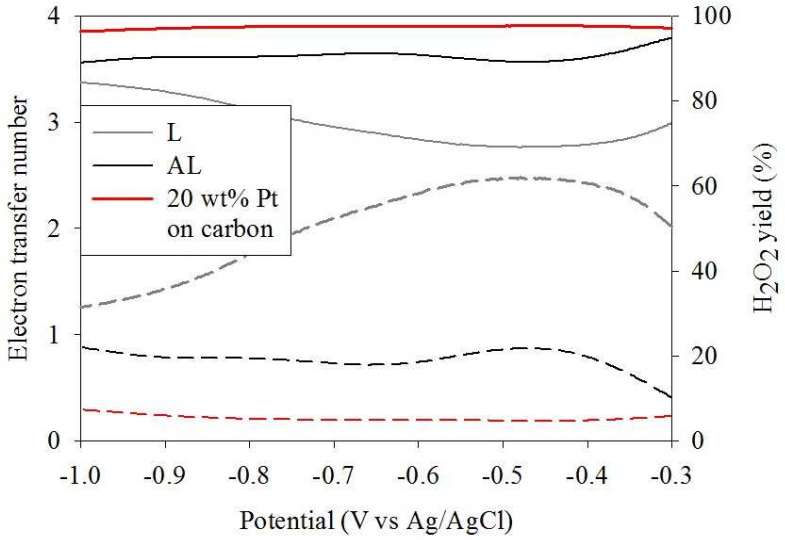

Figure 9. Electron transfer number (full lines) and hydrogen peroxide yield (dotted lines) calculated via RRDE measurements in 0.1 M KOH for Lobster/L (grey), Artificial Lobster/AL (black) and 20 wt% platinum on Vulcan carbon (red).

Stability testing was also carried out for both catalysts as well as the tolerance to methanol crossover in alkaline media (Figure 10). Therefore a chronoamperic response was recorded, where a constant potential was held over 10000 seconds. Both catalysts showed a lower stability than the platinum standard, with a loss in current of 33 % for L, 38 % for AL and only 28 % for the platinum standard. To investigate the methanol tolerance of each sample, 5 mL of methanol was added to the electrolyte after 160 seconds while running the chronoamperic response. Both catalysts showed a higher tolerance to methanol than the platinum standard, where the presence of methanol even seems to increase the stability of AL, ending with a loss of current of 26 % after 1000 seconds, the same as L, whereas the platinum standard shows a considerable loss of 40 %.

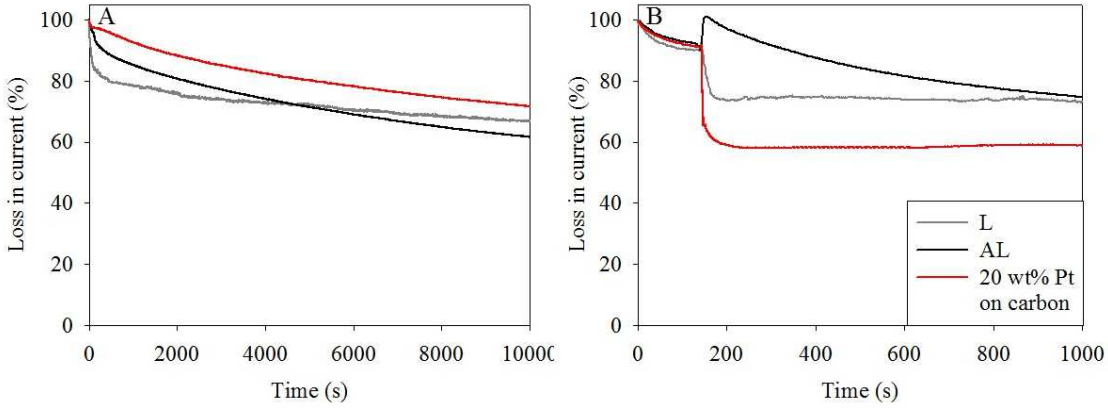

Figure 10. Comparison of the chronoamperic response recorded at a constant rotational speed of 800 rpm and potential of – 0.25 V for A) stability testing over 10000 seconds and B) methanol tolerance over 1000 seconds, where 5 mL of methanol was added after 160 seconds in 0.1 M KOH for Lobster/L (grey), Artificial Lobster/AL (black) and 20 wt% platinum on Vulcan carbon (red).

Considering the above results AL shows good catalytic activity when compared to a commercially

available platinum standard in alkaline media, whereas L performs rather poorly, as expected. This variation in performance can be explained by various crucial differences between the two synthesised catalysts, not only in surface area and pore volume, but also in carbon content and degree of graphitisation as well as the amount of nitrogen incorporated into the carbon framework. It is known that a catalyst`s activity towards the ORR is mostly dependent on the material`s surface area, conductivity and functional groups present on the surface or active sites [37]. With 188 m^2/g AL has a similar surface area to the platinum standard (163 m^2/g) than L (23 m^2/g), though the active sites, playing a crucial role, are completely different. Despite being often discussed, the active sites in nitrogen doped carbons are still not fully understood. A combination of graphitic and pyridinic nitrogen may be favourable, as has been shown by Lai et al. [38], where the limiting current is dependent on the graphitic nitrogen content and pyridinic nitrogen improving the onset potential. Conceptually, graphitic nitrogen has the ability to add one extra electron to the delocalised π-orbitals, whereas the lone pair of free electrons in pyridinic nitrogen increases the basicity or the electron donor capacity of the structure. Regardless of the disagreements in literature, both of these capabilities can ultimately improve a materials` ORR activity, as has recently been discussed in the reviews of Daems et al. [5]and Liu et al.[39]. However, it can be said that the difference in nitrogen content regarding the two synthesised catalysts, 2 wt% for AL and below 0.5 wt% for L, plays a decisive role when it comes to catalytic activity. Considering the total pore volume, where L is basically non porous, AL shows a mixture of micro- and mesopores, which is also crucial for the ORR activity due to the mass transport processes [40]. Though the material`s conductivity has not been investigated in this work, by correlating the degree of graphitisation with the conductivity [41],[42], it can be assumed that AL is more graphitic and thus also more conductive than L due to its higher amount of carbon and lower I_D/I_G value in Raman spectroscopy, again supporting the difference in catalytic performance. Another reason for the lower catalytic activity of L can be the presence of a considerable amount of additional phases such as hydroxyapatite, in contrast to AL with only very little calcium remaining.

4. Conclusions

Two different nitrogen doped electro-catalysts for the oxygen reduction reaction were synthesised by a simple and cheap one-pot method, taking either real lobster shells or a mixture of chitin and calcium carbonate as precursors. Calcium carbonate acts as a pore generator in both samples, though only to a limited extend in the real lobster catalyst, due to an unequal distribution of components. Compositional analysis revealed leftovers of calcium in both catalysts after the final acid treatment, as well as phosphorus and sulphur for the real lobster sample. Electrochemical characterisation in alkaline media resulted in good performance for the chitin/$CaCO_3$ catalyst, with a similar onset potential to a commercially available platinum catalyst and rather poor catalytic activity of the real lobster sample, due to its limited surface area and pore volume. Both catalysts showed no activity in acidic media. Further development and optimisation of the synthesis conditions could improve the catalytic activity of both catalysts, by on the hand completely removing impurities such as calcium, which would result in a higher surface area, and on the other hand by

obtaining a higher degree of graphitisation, which would lead to an improved conductivity.

Acknowledgments

We would like to thank Dr Harshit Porwal from Queen Mary University of London for helping with Raman spectroscopy and the EU for the Intra European Marie Curie Research Fellowship (PIEF-GA-2013-623227).

References:

[1] I. Katsounaros, W.B. Schneider, J.C. Meier, U. Benedikt, P.U. Biedermann, A. a. Auer, K.J.J. Mayrhofer, Phys. Chem. Chem. Phys. 14 (2012) 7384.

[2] L. Zhang, Z. Xia, J. Phys. Chem. C 115 (2011) 11170–11176.

[3] N.M.R. Peres, F. Guinea, A.H. Castro Neto, Phys. Rev. B 73 (2006) 125411.

[4] H. Wang, T. Maiyalagan, X. Wang, ACS Catal. 2 (2012) 781–794.

[5] N. Daems, X. Sheng, I.F.J. Vankelecom, P.P. Pescarmona, J. Mater. Chem. A 2 (2014) 4085.

[6] R.J. White, N. Yoshizawa, M. Antonietti, M.-M. Titirici, Green Chem. 13 (2011) 2428.

[7] L. Zhao, N. Baccile, S. Gross, Y. Zhang, W. Wei, Y. Sun, M. Antonietti, M.-M. Titirici, Carbon N. Y. 48 (2010) 3778–3787.

[8] R.J. White, M. Antonietti, M.-M. Titirici, J. Mater. Chem. 19 (2009) 8645.

[9] S. Chen, J. Bi, Y. Zhao, L. Yang, C. Zhang, Y. Ma, Q. Wu, X. Wang, Z. Hu, Adv. Mater. 24 (2012) 5593–5597.

[10] Y. Shao, J. Sui, G. Yin, Y. Gao, Appl. Catal. B Environ. 79 (2008) 89–99.

[11] S.-A. Wohlgemuth, R.J. White, M.-G. Willinger, M.-M. Titirici, M. Antonietti, Green Chem. 14 (2012) 1515.

[12] N. Fechler, S.-A. Wohlgemuth, P. Jäker, M. Antonietti, J. Mater. Chem. A 1 (2013) 9418.

[13] C.S. Kong, D.-Y. Kim, H.-K. Lee, Y.-G. Shul, T.-H. Lee, J. Power Sources 108 (2002) 185–191.

[14] D. Raabe, P. Romano, C. Sachs, H. Fabritius, a. Al-Sawalmih, S.B. Yi, G. Servos, H.G. Hartwig, Mater. Sci. Eng. A 421 (2006) 143–153.

[15] FAO, Yearb. Fish. Stat. (2013).

[16] P.K. Dutta, J. Duta, V.S. Tripathi, J. Sci. Ind. Res. (India). 63 (2004) 20–31.

[17] H. Yuan, L. Deng, X. Cai, S. Zhou, Y. Chen, Y. Yuan, RSC Adv. 5 (2015) 56121–56129.

[18] Y. Li, H. Zhang, P. Liu, Y. Wang, H. Yang, Y. Li, H. Zhao, Electrochem. Commun. 51 (2015) 6–10.

[19] T.X. Wu, G.Z. Wang, X. Zhang, C. Chen, Y.X. Zhang, H.J. Zhao, Chem. Commun. 51 (2015) 1334–1337.

[20] M.K. Rybarczyk, M. Lieder, M. Jablonska, RSC Adv. 5 (2015) 44969–44977.

[21] Z.-Y. Wu, P. Chen, Q.-S. Wu, L.-F. Yang, Z. Pan, Q. Wang, Nano Energy 8 (2014) 118–125.

[22] B. Aghabarari, M. V. Martínez-Huerta, M. Ghiaci, J.L.G. Fierro, M. a. Peña, RSC Adv. 3 (2013) 5378.

[23] F. Boßelmann, P. Romano, H. Fabritius, D. Raabe, M. Epple, Thermochim. Acta 463 (2007) 65–68.

[24] G. Yang, H. Han, T. Li, C. Du, Carbon N. Y. 50 (2012) 3753–3765.

[25] B. Xu, L. Peng, G. Wang, G. Cao, F. Wu, Carbon N. Y. 48 (2010) 2377–2380.

[26] S. Abdolmohammadi, S. Siyamak, N.A. Ibrahim, W.M.Z.W. Yunus, M.Z.A. Rahman, S. Azizi, A. Fatehi, Int. J. Mol. Sci. 13 (2012) 4508–4522.

[27] P. a. Williamson, P.J. Blower, M. a. Green, Chem. Commun. 47 (2011) 1568–1570.

[28] L. Qing, G. Wu, in:, X. Feng (Ed.), Nanocarbons Adv. Energy Convers., Wiley, 2015, pp. 75–116.

[29] K.V. Kumar, K. Preuss, L. Lu, Z.X. Guo, M.M. Titirici, J. Phys. Chem. C 119 (2015) 22310–22321.

[30] C.H. Choi, S.H. Park, S.I. Woo, Green Chem. 13 (2011) 406–412.

[31] M. Fang, K. Wang, H. Lu, Y. Yang, S. Nutt, J. Mater. Chem. 19 (2009) 7098.

[32] R. Xie, G. Fan, Q. Ma, L. Yang, F. Li, J. Mater. Chem. A 2 (2014) 7880.

[33] R. Bajpai, S. Roy, N. Kulshrestha, J. Rafiee, N. Koratkar, D.S. Misra, Nanoscale 4 (2012) 926–930.

[34] C.C. Silva, a. S.B. Sombra, J. Phys. Chem. Solids 65 (2004) 1031–1033.

[35] C.G. Kontoyannis, N.C. Bouropoulos, P.G. Koutsoukos, Vib. Spectrosc. 15 (1997) 53–60.

[36] M. Shao, in:, M. Shao (Ed.), Electrocatal. Fuel Cells - A Non- Low-Platinum Approach, Springer, 2013, pp. 513–532.

[37] S. Zhang, K. Gong, L. Dai, in:, M. Shao (Ed.), Electrocatal. Fuel Cells A Non- Low- Platin. Approach, Springer, 2013, pp. 375–390.

[38] L. Lai, J.R. Potts, D. Zhan, L. Wang, C.K. Poh, C. Tang, H. Gong, Z. Shen, J. Lin, R.S. Ruoff, Energy Environ. Sci. 5 (2012) 7936.

[39] J. Liu, P. Song, Z. Ning, W. Xu, Electrocatalysis (2015) 132–147.

[40] D. Higgins, C. Zhongwei, in:, M. Shao (Ed.), Electrocatal. Fuel Cells - A Non- Low-Platinum Approach, Springer, 2013, pp. 247–270.

[41] T. Maitra, S. Sharma, A. Srivastava, Y.-K. Cho, M. Madou, A. Sharma, Carbon N. Y. 50 (2012) 1753–1761.

[42] D. Mattia, M.P. Rossi, B.M. Kim, G. Korneva, H.H. Bau, Y. Gogotsi, J. Phys. Chem. B 110 (2006) 9850–9855.